Measurements of Grain Boundary Energy and Anisotropy in Tin

Article *in* Metallurgical and Materials Transactions A · August 2005

DOI: 10.1007/s11661-005-0333-7

2 authors, including:

Peter W Voorhees
Northwestern University
330 PUBLICATIONS **11,471** CITATIONS

SEE PROFILE

Measurements of the Grain Boundary Energy and Anisotropy in Tin

D.J. ROWENHORST and P.W. VOORHEES

The three-dimensional (3-D) geometry of the triple junction formed between two solid Sn-rich particles and a Pb-rich liquid matrix is used to measure the interfacial energy and its anisotropy for individual grain boundaries. The anisotropy is determined using a Cahn–Hoffman capillarity vector analysis of the energy balance at a triple junction. The absolute solid-solid grain boundary energy for each individual boundary is then determined by using the known value for the solid-liquid energy. A total of 136 boundaries are analyzed, with 46 of them forming grain boundaries. The remaining boundaries are found to be wetted boundaries with thin-liquid films formed between the two particles. A correlation between the low interfacial energy and the probability of occurrence for that disorientation is also observed. We also show that the anisotropy, as quantified by the magnitude of the torque term, is a significant portion of the total interfacial energy, especially for low energy boundaries. The degree of twist *vs* tilt of the boundaries is also analyzed. As expected, there are more tilt boundaries within the system than twist boundaries and most of the low energy boundaries have a mixed tilt-twist character.

I. INTRODUCTION

THE interfacial energy of the grain boundaries plays a critical role in the microstructural evolution of the polycrystalline materials.[1] Most models of microstructural evolution assume that the interfacial energy is isotropic. However, many experiments have shown that the grain boundary energy within a system is dependent on the character of the boundary.[2–6] A grain boundary's character, within a centrosymmetric crystal system, can be specified using five macroscopic degrees of freedom (DOF): three DOF to describe the difference in crystallographic orientation between the two crystals, and two more DOF to describe the grain boundary plane. The convention we use here is to describe the difference in crystallographic orientation by a rotation about a unit vector, r, by a misorientation angle ϕ. The grain boundary plane is described by a unit vector, normal to the surface, $\hat{\mathbf{n}}$.

Studies have shown that the variations in grain boundary properties can greatly affect both evolution of the microstructure[7,8] and the properties of the material.[9,10,11] Thus, to understand properly the evolution of the microstructure, information on the relationship between the five macroscopic DOF and the absolute grain boundary energy is needed. It has been calculated that, even after taking into account the crystal symmetry, it would take over 10^5 interfacial energy measurements to completely characterize this parameter space.[12] However, by collapsing some of these DOF into critical parameters, such as the degree of tilt or twist at the boundary, one can gain important and insightful information on the types of boundaries that are present within a system without characterizing all of the possible boundaries within a system.

The Herring relations[13] show that, at a junction between three phases at equilibrium, there must be a balance of forces. This results in the following condition:

$$\sum_{i=1}^{3}\left(\gamma_i\hat{\mathbf{t}}_i + \left(\frac{\partial\gamma}{\partial\theta}\right)_i\hat{\mathbf{n}}_i\right) = 0 \qquad [1]$$

where γ_i is the free energy per unit area of interface, i, and $\left(\frac{\partial\gamma}{\partial\theta}\right)_i$ is the result of the anisotropy in the interfacial energy. This last term describes the energy needed to rotate interface i to a new orientation, and is commonly known as the torque term. By using this relation, the interfacial energy can be experimentally determined by analyzing the geometry of the interfaces at a triple junction.

There are two common ways to measure the grain boundary energies using triple junctions. The first method measures the geometry of the triple junction formed between two grains and a free surface.[2,14] Mykura[14] measured the geometry of grain boundary grooves formed at the surface of pure Sn using interference microscopy. These measurements assumed that the torque terms in Eq. [1] were negligible, and thus were ignored. Also, the crystallographic relationship between the Sn grains was not measured, and only an average value of all grain boundary energies was reported. We will further address this investigation in Section 3.

Gjostein and Rhines[2] also used interference microscopy to measure the grain boundary energies of pure tilt and twist [001] boundaries in copper. Again, during this study, the torque terms were assumed to be small and were ignored. They did find that, at small tilt angles, the energy followed the Read–Shockley behavior,[15] but all the energies reported were relative to the unknown surface energy.

The second method commonly used to measure grain boundary energies is to measure the geometry at the intersection of three grains.[3,4,16] Hasson and Goux measured

D.J. ROWENHORST, former Graduate Research Assistant, Department of Materials Science and Engineering, Northwestern University, is Postdoctoral Researcher, Materials Science and Technology Division, United States Naval Research Laboratory, Washington, DC 20375. P.W. VOORHEES, Frank C. Engelhart Professor, is with the Department of Materials Science and Engineering, Northwestern University, Evanston, IL 60208-3108. Contact e-mail: p-voorhees@northwestern.edu

Manuscript submitted October 5, 2004.

triple junctions formed between [001] and [011] tilt and twist boundaries in pure Al. They found that there are specific boundary orientations with large tilt angles (>10 deg) that displayed lower than expected energies. These special boundaries, commonly called sigma boundaries, are associated with a high degree of atomic site matching at the boundaries. Again, the anisotropy of the boundary was ignored and only relative energies were reported.

Mori *et al*. investigated the triple junction between two Cu grains, and SiO_2 precipitates pinned along the grain boundaries. Only [001] twist boundaries were investigated, and only relative energies were reported, but the study did identify several sigma boundaries that were not detected in the study by Gjostein and Rhines.[2]

The most complete study to date of grain boundary energies as a function grain boundary character has been performed by Saylor *et al*.[5,6] The energy and grain orientations of more than 4×10^6 boundaries were measured in MgO using a combination of serial sectioning and electron backscattering detection. They found that there was a preference for tilt boundaries within the system and for boundaries with at least one [001] normal, and that the energy of these normals was lower than average. However, because there was no reference energy for the system, only relative energies were reported. What is clear from all of the studies of grain boundary energy as a function of the grain orientations is that the grain boundary energy is a function of the specific grain boundary character.

This investigation examines the grain boundary energy of Sn-rich particles randomly dispersed within a Pb-Sn eutectic liquid matrix. This system has been identified as an ideal system for analyzing particle coarsening, and there have been extensive studies characterizing the evolution of the microstructure.[17,18,19] However, if more detailed studies are to be carried out, especially in regimes where there are a substantial number of particle-particle contacts, the grain boundary energies for the system must be characterized.

The grain boundary energy between two contacting Sn-rich particles can be determined by analyzing the triple junction formed by the two Sn-rich crystals and the Pb-Sn eutectic liquid. The earlier investigations into grain boundary energies have been limited to reporting only relative energies, because the Herring relations only provide the relative energy balance at the triple junction. For the solid-state systems studied so far, there is no available reference interfacial energy, either at the surface or in the bulk. However, unlike in many solid-state systems, there have been careful experiments in Pb-Sn solid-liquid systems that measured the solid-liquid interfacial energy to 14 pct. Other experiments that examine liquid inclusions in the solid particles show that the inclusion is nearly spherical, indicating that the solid-liquid interfacial energy is very nearly isotropic. This result is consistent with low volume fraction, long time coarsening experiments preformed in space that show that solid particles in a liquid are very spherical.[19,20] Thus, we are not limited to only reporting relative grain boundary energies, but can experimentally determine the absolute grain boundary energy and anisotropy.

While the solid-liquid interfacial energy is nearly isotropic, the grain boundary energy in general is anisotropic. In the analysis of Herring, the torque term, which is induced by the anisotropic interfacial energy, is only considered to act within a two-dimensional (2-D) plane perpendicular to the triple junction line. However, in our case the interface exists within a three-dimensional (3-D) space, and as such, the torque term will in general not act within the 2-D plane that is normal to the triple junction line. Thus, we will employ the capillarity vector analysis of the triple junction, introduced by Hoffman and Cahn.[21,22] This analysis identifies the total torque term of the boundary and its direction in three dimensions. One consequence of the grain boundary torque is that if the triple junction line is curved, as it is in this system, the dihedral angle formed between the solid-liquid interfaces can vary as a function of position along the triple junction line.

Therefore, this method requires the characterization of the 3-D triple junction geometry. By analyzing the 3-D triple junction, we avoid any artifacts of analysis using a 2-D section, such as those that occur when the sectioning plane is not perpendicular to the grain boundary plane or the triple junction line. The 3-D geometry is determined by first collecting 2-D serial sections of the microstructure. These sections are then aligned and stacked into a 3-D reconstruction of the solid-liquid particles near the triple junction. This also will provide the direction of the grain boundary normal. The crystallographic misorientation between the two Sn crystals is determined using electron backscattering diffraction (EBSD). By analyzing the 3-D geometry and crystallographic information, we can determine the absolute grain boundary energy as a function of all five macroscopic DOF.

II. EXPERIMENTAL METHOD

The samples were cast and cold worked using the method prescribed by Hardy and Voorhees.[17] Since impurities can greatly affect the interfacial energies in an alloy system, 99.99 pct Sn and 99.999 pct Pb were used for producing the samples. The alloy composition was chosen so that, when the sample was heated just above the eutectic temperature, there would be 80 vol pct fraction Sn particles dispersed in a Pb-Sn eutectic liquid. The samples were then heat treated isothermally at 185 °C, just above the eutectic temperature ($T_{\text{eutectic}} = 183$ °C), yielding an interconnected network of Sn particles, as seen in Figure 1. At the end of the coarsening time, the samples were quenched to freeze the eutectic liquid.

Two samples were used for this investigation. The first was coarsened for 48 hours. This gives a sufficiently large average particle size that the triple junction geometry was easily resolved. The second sample was coarsened for 24 hours to increase the number of grain boundaries collected. Previous investigations have shown that the initial particle size for the samples is approximately 10 μm, as measured on 2-D sections, at the beginning of the heat treatment.[19] During the heat treatment, due to particle coarsening, the larger particles will grow at the expense of the smaller particles, thus increasing the average particle size. During the coarsening process, the new material deposited on the particles, including that at the grain boundaries, is at the equilibrium concentration of solid in contact with eutectic liquid. This implies that the solid contains 1.3 at. pct Pb. This processing path ensures that the triple junctions are at an equilibrium state.

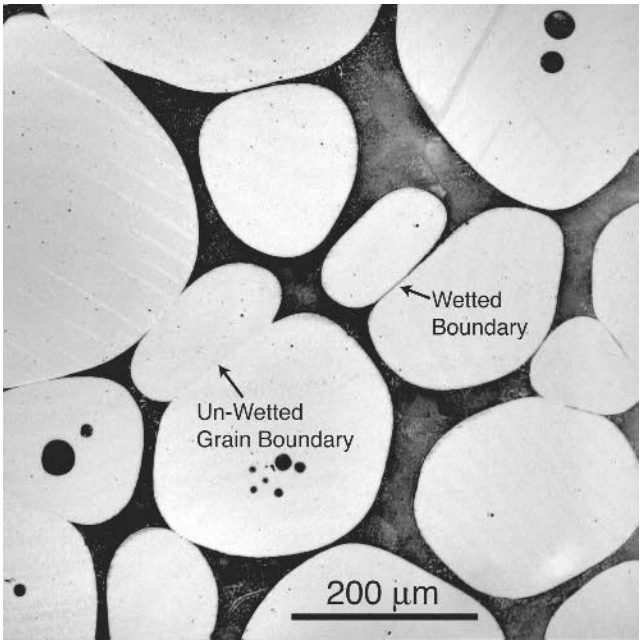

Fig. 1—Representative micrograph of one of the serial sections. The lighter regions are the solid tin-rich particles and the dark phase is the Pb-Sn eutectic phase. Examples of a wetted and nonwetted grain boundary are given. Notice the thin-liquid film formed between the two particles of the wetted boundary. The dark areas inside the particles are liquid droplets that become trapped inside the particles.

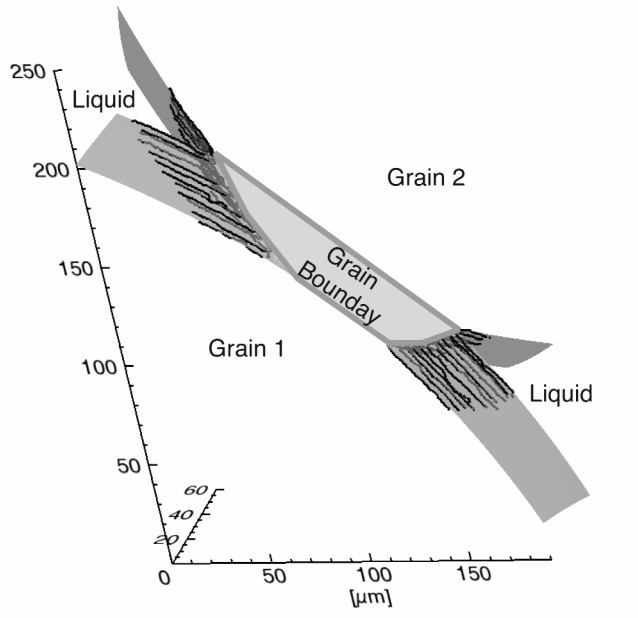

Fig. 2—3-D rendering of two triple junctions on either side of a grain boundary. The black points are the actual positions of the solid-liquid interface. The four dark gray surfaces are the ellipsoidal fits to the data. The grain boundary plane is assumed to be the plane defined by the two intersections of the ellipsoidal fits, and is shown in light gray.

The 3-D geometry of the triple junctions was determined using serial sections that were taken of the sample using the method described by Alkemper and Voorhees.[23] In this method, an optical microscope is connected directly to the sectioning machine, eliminating any tilt or rotation alignment uncertainties from mounting and dismounting the sample. The translation misalignment of the images of the sections only occurs in one direction and is accurately measured using a linear variable differential transformer (LVDT). The images are acquired using an optical microscope equipped with a high-resolution digital camera. The resultant lateral resolution within each of the 2-D sections is 1.10 μm.

For this analysis, the spacing between sections was 4.75 μm. Each analyzed grain boundary contained at least five sections, while the average number of sections was typically eight. Using the data from the LVDT, the images were then aligned and stacked using a computer program. The interface between the Sn particles and the Pb-Sn eutectic was determined by thresholding the grayscale images.

The boundaries that were analyzed were chosen such that there were two triple junctions on either end of a grain boundary. The grain boundaries had to span at least five sections in order to resolve properly the curvature of the triple line in the sectioning direction. Also, both particles had to be present in the last section so that the crystal orientation could be determined using EBSD.

The locations of the grain boundaries were entered into a surface fitting program to determine the geometry of the triple junction. Each point along the solid-liquid interface in the stack of images was assigned to one side of each of the two triple junctions. This gives us the position, in three dimensions, of two interfaces for each of the two triple junctions, for a total of four interfaces. Each one of these four interfaces is then fitted to a portion of an ellipsoidal surface, as seen in Figure 2.

While the complete shape of the entire particle is not well described by a single ellipsoid, the curvature and shape of the interface near the triple junction is well described by an ellipsoid. For this reason, only the 30 μm of the interfaces nearest to the triple junction were considered for the ellipsoid fit. To verify that there were no size affects associated with our measurement technique, sample boundaries from the 48 hours sample were analyzed twice, once at full resolution and once with a reduced resolution, simulating the smaller particle size of the sample processed for 24 hours. We found no change in the results.

The exact position of the triple junctions was determined by numerically solving for the intersection between the two ellipsoid surfaces. The grain boundary plane is given by the plane of best fit of the two triple-junction lines. Bending or twisting of the grain boundary was not observed in the reconstructions of the 3-D triple junctions, which indicates that the grain boundary normal is constant for the triple junction. This then provides a mathematical description of the geometry of the interfaces at the triple junction, as well as the grain boundary normal.

Finally, the crystallographic orientations of each particle are determined using EBSD. The sample is mounted on a sample holder that allows for the sample to be moved directly from the serial sectioning machine to the scanning electron microscope (SEM). This reduces errors that would occur when the sample is unmounted and remounted to another holder. Since each particle is a single crystal,[24] the crystal

orientation of each particle is determined by taking a Kikuchi pattern from one point on the particle near the grain boundary. The pattern is then automatically indexed using the EBSD software, providing the orientation of each crystal relative to the sample coordinate system. From the two crystal orientations, the misorientation and the disorientation are determined for the boundary. The misorientation angle is the minimum angle needed to rotate one crystal into the second crystal orientation, about an arbitrary axis that is common to both crystals. However, because the crystal contains symmetry, there are many equivalent misorientations. In the tetragonal crystal system, there are eight proper symmetry operations for each crystal. Also, the misorientation can be described by rotating crystal A to B or B to A. Therefore, there are $8 \times 8 \times 2 = 128$ equivalent misorientations for each boundary. The disorientation is simply the misorientation that provides the minimum rotation angle, and whose rotation vector is contained within the crystallographic unit triangle for the tetragonal system. The error in detecting the absolute orientation of each crystal, caused mainly by the necessity of moving the sample from the serial sectioning machine to the SEM, is approximately 6 deg, which will then be the error in the crystallographic orientation of the grain boundary normal. Because the disorientation is measured from one crystal to the second, and is not relative to the sample coordinate system, the error in the disorientation measurements is only 1 deg.

Capillarity Vector Analysis

As mentioned previously, the Herring relation[13] states that, at the triple junction between grains 1, 2, and 3, the balance of the forces implies that the interfacial energies and torque terms are related as given in Eq. [1]. The limitation of this notation is that the Herring relation ignores that the torque term is not a constant along a triple junction in three dimensions, but rather it is dependent on the particular direction of $\hat{\mathbf{t}}$.

Cahn and Hoffman[21,22] introduced the capillarity vector, $\boldsymbol{\xi}$, that can account for the nonconstant torque energy along a triple junction. The capillarity vector is related to the interfacial energy, γ, by

$$(\boldsymbol{\xi} \cdot \hat{\mathbf{n}})\hat{\mathbf{n}} = \boldsymbol{\xi}_n = \gamma\hat{\mathbf{n}} \qquad [2]$$

where $\boldsymbol{\xi}_n$ is the component of $\boldsymbol{\xi}$ normal to the interface plane. The magnitude of the maximum torque for the boundary, $\frac{\partial\gamma}{\partial\theta_{\max}}$, is given by

$$\boldsymbol{\xi} - \boldsymbol{\xi}_n = \boldsymbol{\xi}_{t_0} = \frac{\partial\gamma}{\partial\theta_{\max}}\hat{\mathbf{t}}_0 \qquad [3]$$

where $\boldsymbol{\xi}_{t_0}$ is the component of $\boldsymbol{\xi}$ contained within the interface plane, and $\hat{\mathbf{t}}_0$ is the unit vector that gives the direction of the maximum angular rate of change of γ. This term is the energy to rotate the normal to the interface plane, $\hat{\mathbf{n}}$, in the direction of $\hat{\mathbf{t}}_0$. For any other tangent vector in the boundary plane, $\hat{\mathbf{t}}$, the resolved torque, $\frac{\partial\gamma}{\partial\theta}$, is given by

$$\frac{\partial\gamma}{\partial\theta} = \boldsymbol{\xi}_{t_0} \cdot \hat{\mathbf{t}} = \frac{\partial\gamma}{\partial\theta_{\max}}\cos\psi \qquad [4]$$

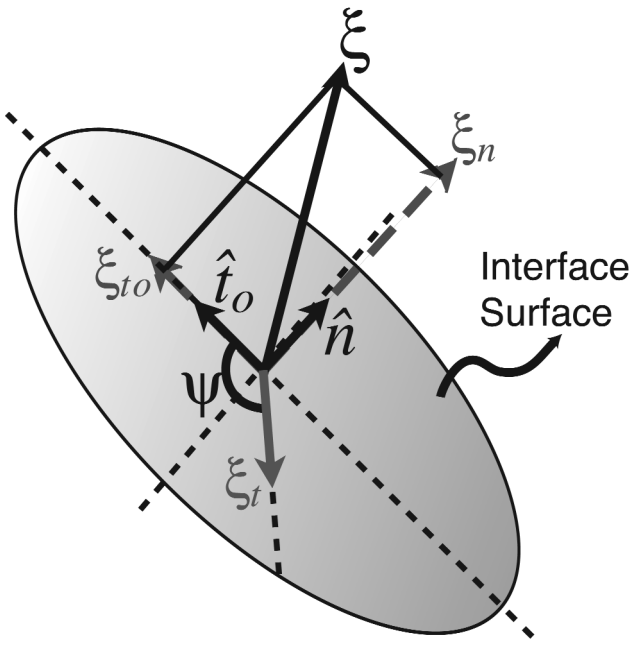

Fig. 3—A schematic showing the relation between an interface, the capillarity vector, $\boldsymbol{\xi}$, the maximum torque term, $\boldsymbol{\xi}_{t_0}$, and the resolved torque term, $\boldsymbol{\xi}_t$.

where ψ is the angle between $\hat{\mathbf{t}}_0$ and $\hat{\mathbf{t}}$, (Figure 3).

Cahn and Hoffman show that the energy balance at a triple junction in terms of the capillarity vector is given by

$$(\boldsymbol{\xi}^{12} + \boldsymbol{\xi}^{23} + \boldsymbol{\xi}^{31}) \times \hat{\mathbf{l}}^{123} = 0 \qquad [5]$$

where $\boldsymbol{\xi}^{ij}$ is the capillarity vector between interface i and j and $\hat{\mathbf{l}}^{123}$ is the unit vector along the triple junction.

The solid-liquid interfacial energy in the Pb-Sn system is, to a good approximation, isotropic; thus, the triple junction has two isotropic solid-liquid interfacial energies given by $\boldsymbol{\xi}^{SL}$ and $\boldsymbol{\xi}^{LS}$, and an anisotropic grain boundary energy given by $\boldsymbol{\xi}^{12}$ (Figure 4). The interfacial balance for this triple junction is given by

$$(\boldsymbol{\xi}^{SL} + \boldsymbol{\xi}^{LS} + \boldsymbol{\xi}^{31}) \times \hat{\mathbf{l}}^{12L} = 0 \qquad [6]$$

where $\hat{\mathbf{l}}^{12L}$ is the triple-junction unit vector, which is perpendicular to all three surface normals. We know that the solid-liquid interfacial energy is very nearly isotropic, so we will assume that $\left(\frac{\partial\gamma}{\partial\theta}\right)_{\max} = 0$. This means that the direction of $\boldsymbol{\xi}^{LS}$ and $\boldsymbol{\xi}^{SL}$ is given by the normal to the solid-liquid surface. Thus, the only unknowns are the magnitude and direction of $\boldsymbol{\xi}^{12}$.

To solve for the energy of the grain boundary, we express $\boldsymbol{\xi}^{12}$, $\boldsymbol{\xi}^{SL}$, and $\boldsymbol{\xi}^{LS}$ within the coordinate system defined by $\hat{\mathbf{n}}^{12}$, $\hat{\mathbf{t}}^{12}$, and $\hat{\mathbf{l}}^{12l}$. Rewriting Eq. [6] in terms of this coordinate system, we have

$$(\boldsymbol{\xi}^{SL} \cdot \hat{\mathbf{n}}^{12} + \boldsymbol{\xi}^{LS} \cdot \hat{\mathbf{n}}^{12} + \boldsymbol{\xi}^{12} \cdot \hat{\mathbf{n}}^{12})\hat{\mathbf{n}}^{12} \times \hat{\mathbf{l}}^{12L} + (\boldsymbol{\xi}^{SL} \cdot \hat{\mathbf{t}}^{12} + \boldsymbol{\xi}^{LS} \cdot \hat{\mathbf{t}}^{12} + \boldsymbol{\xi}^{12} \cdot \hat{\mathbf{t}}^{12})\hat{\mathbf{t}}^{12} \times \hat{\mathbf{l}}^{12L} + (\boldsymbol{\xi}^{SL} \cdot \hat{\mathbf{l}}^{12L} + \boldsymbol{\xi}^{LS} \cdot \hat{\mathbf{l}}^{12L} + \boldsymbol{\xi}^{12} \cdot \hat{\mathbf{l}}^{12L})\hat{\mathbf{l}}^{12L} \times \hat{\mathbf{l}}^{12L} = 0 \qquad [7]$$

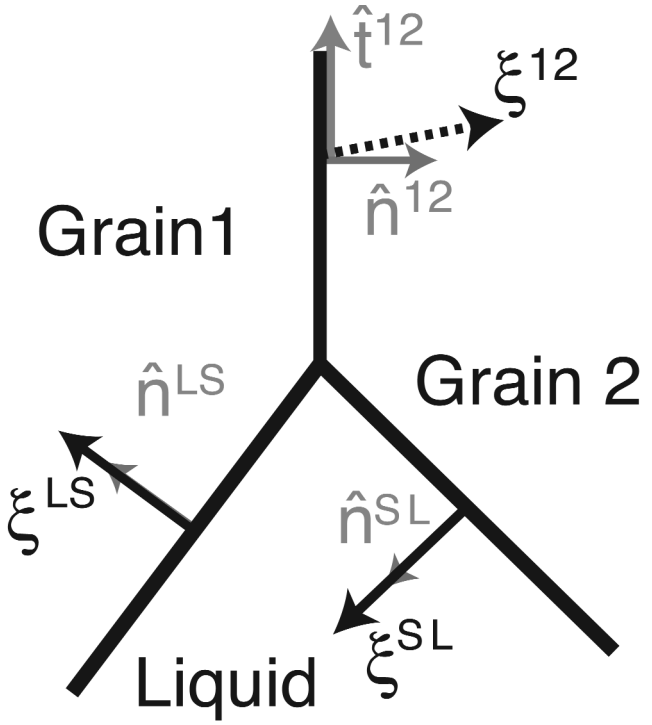

Fig. 4—Diagram of a triple junction between two grains within a liquid matrix with an isotropic interfacial energy. The triple-junction unit vector, $\hat{\mathbf{l}}^{12L}$, is perpendicular to the diagram. The capillarity vector for the grain boundary, $\boldsymbol{\xi}^{12}$, is anisotropic; thus, there is a component of $\boldsymbol{\xi}^{12}$ that is contained within the plane defined by $\hat{\mathbf{t}}$ and $\hat{\mathbf{l}}^{12L}$ but in general is not necessarily parallel to $\hat{\mathbf{l}}^{12L}$ or $\hat{\mathbf{t}}$.

The last term, $(\boldsymbol{\xi}^{12} \cdot \hat{\mathbf{l}}^{12L})\hat{\mathbf{l}}^{12L} \times \hat{\mathbf{l}}^{12L}$ is equal to zero, since $\hat{\mathbf{l}}^{12L} \times \hat{\mathbf{l}}^{12L} = 0$. Furthermore, the normal vectors of the solid-liquid interfaces, and thus $\boldsymbol{\xi}^{SL}$ and $\boldsymbol{\xi}^{LS}$, are contained within the plane defined by $\hat{\mathbf{n}}^{12}$ and $\hat{\mathbf{t}}^{12}$. This means that $\boldsymbol{\xi}^{SL} \cdot \hat{\mathbf{l}}^{12L}$ and $\boldsymbol{\xi}^{LS} \cdot \hat{\mathbf{l}}^{12L}$ are both equal to zero. Since $\hat{\mathbf{n}}^{12} \times \hat{\mathbf{l}}^{12L}$ and $\hat{\mathbf{t}}^{12} \times \hat{\mathbf{l}}^{12L}$ are perpendicular to each other, their sum cannot be equal to zero. Therefore, Eq. [7] implies

$$\boldsymbol{\xi}^{SL} \cdot \hat{\mathbf{n}}^{12} + \boldsymbol{\xi}^{LS} \cdot \hat{\mathbf{n}}^{12} + \boldsymbol{\xi}^{12} \cdot \hat{\mathbf{n}}^{12} = 0 \qquad [8a]$$

$$\boldsymbol{\xi}^{SL} \cdot \hat{\mathbf{t}}^{12} + \boldsymbol{\xi}^{LS} \cdot \hat{\mathbf{t}}^{12} + \boldsymbol{\xi}^{12} \cdot \hat{\mathbf{t}}^{12} = 0 \qquad [8b]$$

Using Eqs. [2] and [4], we can rewrite these sums as

$$\boldsymbol{\xi}^{SL} \cdot \hat{\mathbf{n}}^{12} + \boldsymbol{\xi}^{LS} \cdot \hat{\mathbf{n}}^{12} + \gamma = 0 \qquad [9a]$$

$$\boldsymbol{\xi}^{SL} \cdot \hat{\mathbf{t}}^{12} + \boldsymbol{\xi}^{LS} \cdot \hat{\mathbf{t}}^{12} + \left(\frac{\partial \gamma}{\partial \theta}\right)_{\max} \cos \psi = 0 \qquad [9b]$$

We can now directly solve for the interfacial energy, γ, which, by the definition in Eq. [2], is the magnitude of $\boldsymbol{\xi}_n^{12}$. We can also solve for $\left(\frac{\partial \gamma}{\partial \theta}\right)_{\max}$, which, as stated in Eq. [3], is related to the tangential component of the capillarity vector term at that point on the boundary. Assuming that the energetics of the boundary are constant for the boundary, and that the normal of the grain boundary plane is the same at all points along the triple junction, the maximum torque term can be determined by solving the interface balance at two different points along the triple junction located at $\hat{\mathbf{t}}_2$ and $\hat{\mathbf{t}}_1$. If $\Delta\psi$ is the angle from $\hat{\mathbf{t}}_2$ to $\hat{\mathbf{t}}_1$ and ψ_1 is the unknown angle from $\hat{\mathbf{t}}_1$ to $\hat{\mathbf{t}}_0$, then we solve the set of equations:

$$\left(\frac{\partial \gamma}{\partial \theta}\right)_{\max} \cos \psi_1 = \left(\frac{\partial \gamma}{\partial \theta}\right)_{t_1} \qquad [10a]$$

$$\left(\frac{\partial \gamma}{\partial \theta}\right)_{\max} \cos (\psi_1 + \Delta\psi) = \left(\frac{\partial \gamma}{\partial \theta}\right)_{t_2} \qquad [10b]$$

for $\left(\frac{\partial \gamma}{\partial \theta}\right)_{\max}$ and ψ_1, where $\left(\frac{\partial \gamma}{\partial \theta}\right)_{t_i}$ is the magnitude of the anisotropy at the given tangent direction. The magnitude of $\boldsymbol{\xi}_{t_0}^{12}$ is given by $\left(\frac{\partial \gamma}{\partial \theta}\right)_{\max}$ and the direction of $\boldsymbol{\xi}_{t_0}^{12}$ is given by the angle ψ_1

The accuracy of this analysis was tested by using computer constructed microstructures with a known geometry at the triple junction. These microstructures were constructed so that they had the same degree of error in defining the location of the solid-liquid interface as was found in the real microstructures. We found that there was less than a 1 pct error in defining interfacial energy. The error in defining magnitude of the maximum torque term was 12 pct of the solid-liquid interfacial energy.

By determining the magnitude and direction of $\boldsymbol{\xi}_n^{12}$ and $\boldsymbol{\xi}_{t_0}^{12}$, we have solved for a complete energy of a given grain boundary. All that is needed is to determine the solid-liquid interface normals and the grain-boundary normal at the triple junction. These are easily found from the ellipsoidal fits of the interfaces. The absolute grain boundary energies can be determined by using the measurements of the solid-liquid energy, as given by Gündüz and Hunt.[25] They found that the Sn-eutectic interfacial energy is 132.43 ± 18.94 mJ/m^2. It should be noted that this error will only affect the absolute grain boundary energies, not their relative energies.

III. RESULTS

A total of 138 grain boundaries were analyzed. Of these, 92 were determined to be wetted boundaries, meaning that their grain boundary energy is greater than twice the solid-liquid energy. The determination of a wetted boundary was made by looking for thin liquid films that form between two particles. An example of a thin liquid film is shown in Figure 1. A boundary was considered wetted after a thin liquid film was observed in all sections in which the two particles exist. There had to be five or more sections through a particular grain boundary. While misorientations for the wetted boundaries can easily be determined using EBSD, the grain boundary normal cannot be determined since the geometry between the two particles does not provide a definite normal plane at the wetted surfaces. This also means that the grain boundary energy cannot be determined for the wetted boundaries, but a lower bound can be set as the energy needed to form the two solid-liquid interfaces.

In Figure 5, the two separate components of $\boldsymbol{\xi}$, the interfacial energy (γ), and the maximum torque ($\partial\gamma/\partial\theta_{\max}$) are plotted *vs* the disorientation angle, between the two crystals. Notice that the maximum disorientation for the tetragonal crystal system is 98.42 deg, as opposed to a cubic system

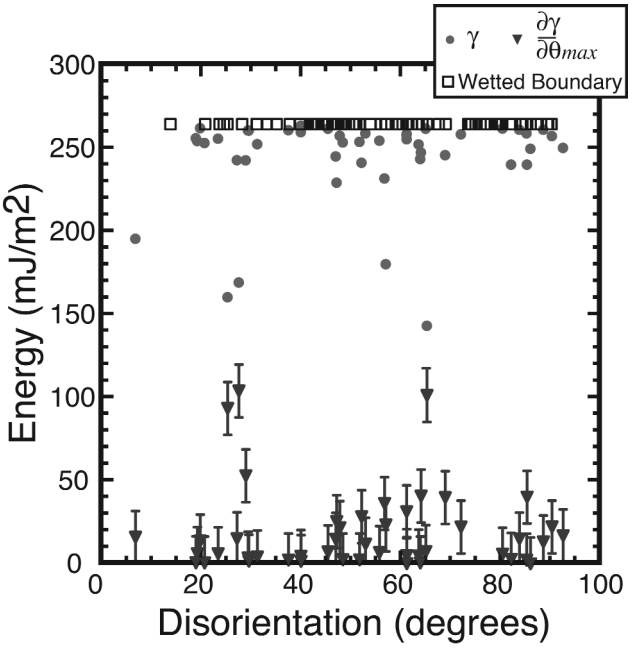

Fig. 5—Grain boundary energy and the maximum torque energy plotted *vs* the disorientation angle between the two crystals. The error bars on the interfacial energy, γ, are smaller than the plotted points. The wetted boundaries are also plotted, which have an energy equal to or greater than twice the solid-liquid interfacial energy.

where the maximum disorientation angle would be 62.8 deg.[26] The wetted boundaries are also represented on this plot by the open squares, and are plotted to provide a lower bound of the wetted boundary energy. These grain boundaries have energies that are larger than or equal to $2\gamma_{SL} = 265$ mJ/m^2, but cannot be experimentally determined since the boundary is wetted.

While much of the data is scattered, we can make some general observations. First notice that most of the grain boundaries have an interfacial energy, γ, that is greater than 200 mJ/m^2. There are a few exceptions, with five boundaries that have an interfacial energy significantly less than this, with disorientation angles near 6, 25, 27, 57, and 65 deg. Previous studies performed by Wolfsdorf-Brenner *et al.*[24] investigated the disorientation probability between neighboring Sn particles in the Pb-Sn system. They found that there was an increase in the probability, when compared to a random distribution, at the same disorientation angles at which we observe the lower interfacial energies. Other investigations into the creep behavior of Sn-Ag alloys[27] identified coincident site lattice (CSL) models for pure Sn crystals with disorientations of 22.3, 43, and 71 deg, and twin relationships at disorientations of 59 and 62 deg. While the disorientations of these models do not exactly agree with the disorientations of the lower energy boundaries, it is important to note that one would expect boundaries close in misorientation to these special boundaries to also have a lower energy, displaying a Read–Shockley type behavior near cusp orientations.[3,15,16] Also, the models do not account for the any solute segregation to the grain boundaries, which may lead to changes in the misorientation of the CSL and twin boundary models.

It is important to note that there are high energy and wetted boundaries at the same disorientations where we observe the lower energy boundaries. Remember that the disorientation angle only represents one of the five DOF of a grain boundary; thus, two given boundaries may have the same disorientation angle, but a very different grain boundary structure. Therefore, the relationship between the disorientation angle and the interfacial energy is unclear. However, our results are consistent with other grain boundary studies that sampled a much larger population of grain boundaries as a function of all five macroscopic DOF and found that there is an inverse relationship between the grain boundary energy and the relative population of the grain boundary, so that there are more lower energy boundaries within the system than is predicted by a system with a random distribution of grain orientations.[5,6]

Earlier studies of surface grain boundary grooves in pure Sn have reported an average grain boundary energy of 160 mJ/m^2.[14,28] This is considerably less than the values presented here, where we find only two boundaries with this energy or lower, and with many with energies greater than $2\gamma_{SL}$. Using the Herring relations, we can calculate the average dihedral angle between two Sn-rich particles within the Pb-Sn system. Using the grain boundary energy from these earlier studies, one would expect an average dihedral angle of 105 deg. A simple observation of even the 2-D sections show that this dihedral angle is not the average value in the solid-liquid system. There are two explanations for this discrepancy. The first is that the wire creep experiments performed by Greenhill and McDonald[28] that related the surface energy to grain boundary energy probably did not have a random orientation of Sn crystals, and the samples contained a large number of low energy boundaries. The other source of error, originally mentioned by Mykura,[14] is that the surface energy measurements are altered by the presence of surface oxide formation. In our experiments, the samples are not pure Sn, but Sn with 1.3 at pct Pb. If Pb were to segregate to the boundary, this would lower the energy of the boundary, not raise it. Thus, the discrepancy is likely the presence of texture in the wires or oxide formation at the surfaces.

The maximum torque, $(\partial\gamma/\partial\theta)_{\max}$, is also plotted in Figure 5. We can see that, for most boundaries, the maximum torque is relatively small compared to the interfacial energy. However, for those boundaries with lower interfacial energies, $(\partial\gamma/\partial\theta)_{max}$, is larger. This inverse relationship is shown more clearly in Figure 6. Previous investigations[2,3,29] found that the interfacial energy decreases rapidly near specific orientations where the boundary assumes a low energy configuration. Thus, we would expect that the magnitude of the maximum torque near these special orientations would increase. Also note that the magnitude of the torque can be a significant fraction of the total energy of a boundary, especially for low grain boundary energies, and should not be ignored. The torque of a boundary will result in variations in the dihedral angle as a function of position along the triple line. For the boundaries with interfacial energies below 170 mJ/m^2, using the capillarity vector analysis, we find that dihedral angle will vary from 106 to 89.9 deg, assuming that the average grain boundary energy is 158 mJ/m^2 and the average torque is 99 mJ/m^2. For the remaining grain boundaries with energies above 170 mJ/m^2, using an average interfacial energy of 250 mJ/m^2 and the average torque of 13.5 mJ/m^2, we find that the dihedral angle between the

particles is 37 deg with a variation in the dihedral angle less than 0.5 deg. This shows the importance of including the torque term, especially when analyzing boundaries with low energies.

Since the grain boundary normal for each nonwetted boundary has also been collected, we can expand our analysis to more than just the disorientation between the crystals. In Table I, we show the crystallographic data for the five low energy boundaries. However, it is extremely difficult to represent the six-dimensional space needed to describe the interfacial energy as a function of the five DOF in a meaningful way. In Figure 7, we construct a 3-D plot, where the interfacial energy of the nonwetted boundaries is plotted *vs* the disorientation angle, and the angle α, which is defined as the angle between the disorientation axis and the grain boundary normal.[31] This effectively folds the two DOF from the grain boundary normal and the two DOF from the misorientation axis into one parameter, α, so that

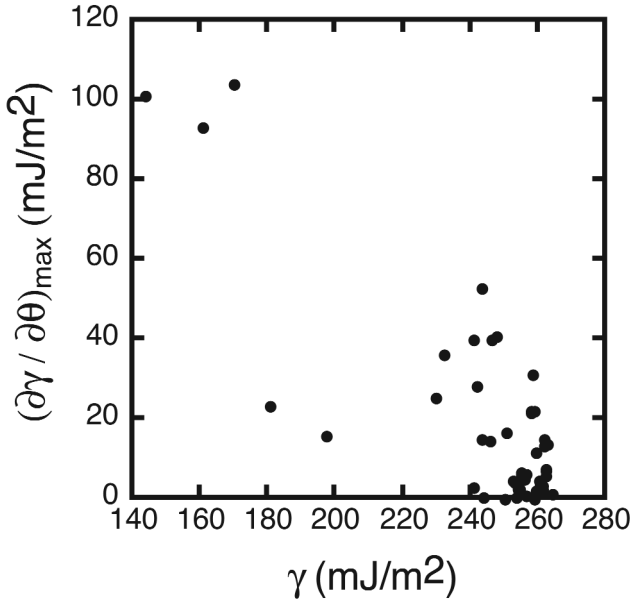

Fig. 6—Plot of the maximum torque term, $\left(\frac{\partial\gamma}{\partial\theta}\right)_{max}$ as a function of the interfacial energy, γ.

$\alpha = 0$ deg represents a pure twist boundary and $\alpha = 90$ deg represents a pure tilt boundary. Values in between these limits represent a mixed twist-tilt boundary. While this approach does not fully represent all five DOF, it does provide further insight into the dependence of the grain boundary energy on the DOF.

Figure 7(a) shows that there are a greater number of near-tilt boundaries in this system than near-twist boundaries. Morawiec has shown that the probability, p, of finding a particular value of α is simply given by the probability of finding the angle between an arbitrary unit vector representing the grain boundary normal and randomly chosen unit vector that represents the misorientation axis, which is given by $p(\alpha) = \sin(\alpha)$.[30] This calculated probability is also plotted in Figure 7(b). We observe a reasonable agreement between the prediction and the experimental data, even with the limited statistics present in the experimental data. It has been shown that the Sn particles are not oriented randomly, and the system has a small amount of crystallographic texture,[32] which may affect the relative populations of tilt or twist boundaries. It is also important to note that the wetted boundaries are not represented here because the grain boundary normal for these boundaries cannot be properly defined; thus, we cannot be sure if these boundaries would affect the distribution of alpha.

The tilt-twist character can also provide us with further insight into the lower energy boundaries. From Figure 5, it appears that the low interfacial energy measurements near 26 deg belong to a single cusp orientation. These two boundaries are represented on Figure 7 by the two darkest points with a disorientation near 26 deg. We see that these two boundaries are very different, with one being nearly a pure tilt boundary and the other with a mixed tilt-twist character. This shows that, for *a*, the distribution of grain boundaries in our experiment, the disorientation between two particles is not sufficient to quantify the energy between them. Figure 7 also shows that the other three low energy boundaries have a mixed tilt-twist character near $\alpha \approx 60$ deg. The data from Table I do not show any clear relation as to why these boundaries display a lower energy. However, because of the low number of low energy boundaries, it is difficult to determine the effect of the grain boundary normal on the interfacial energy. Also, the low energy of these boundaries may be due to Pb enrichment at the boundary,

Table I. Grain Boundary Crystallographic Data, Interfacial Energy, and Maximum Torque Component for Boundaries with an Interfacial Energy Less Than 200 mJ/m^2 (All Directions Are Given in the Crystal Coordinate System, and the Disorientation Vector is Defined from the First Crystal Normal)

Disorientation Angle (deg)	Disorientation Vector, **r**	Grain Boundary Normal, $\mathbf{n}_1$,$\mathbf{n}_2$	γ (mJ/m^2)	$(\partial\gamma/\partial\theta)_{max}$ (mJ/m^2)
6.57	[0.702 0.630 0.331]	[0.324 −0.440 0.837] [0.401 −0.354 0.8455]	197	18.4
25.0	[0.995 0.0880 0.0417]	[0.234 −0.334 −0.913] [0.289 −0.395 0.872]	161	93.6
27.3	[0.706 0.386 0.594]	[−0.694 −0.710 −0.119] [−0.321 0.910 0.262]	170	104
56.8	[0.700 0.673 0.239]	[−0.0612 0.992 −0.114] [0.683 −0.641 −0.351]	181	23.4
65.0	[0.142 0.987 0.0810]	[0.782 −0.588 −0.204] [−0.473 −0.788 0.393]	143	101

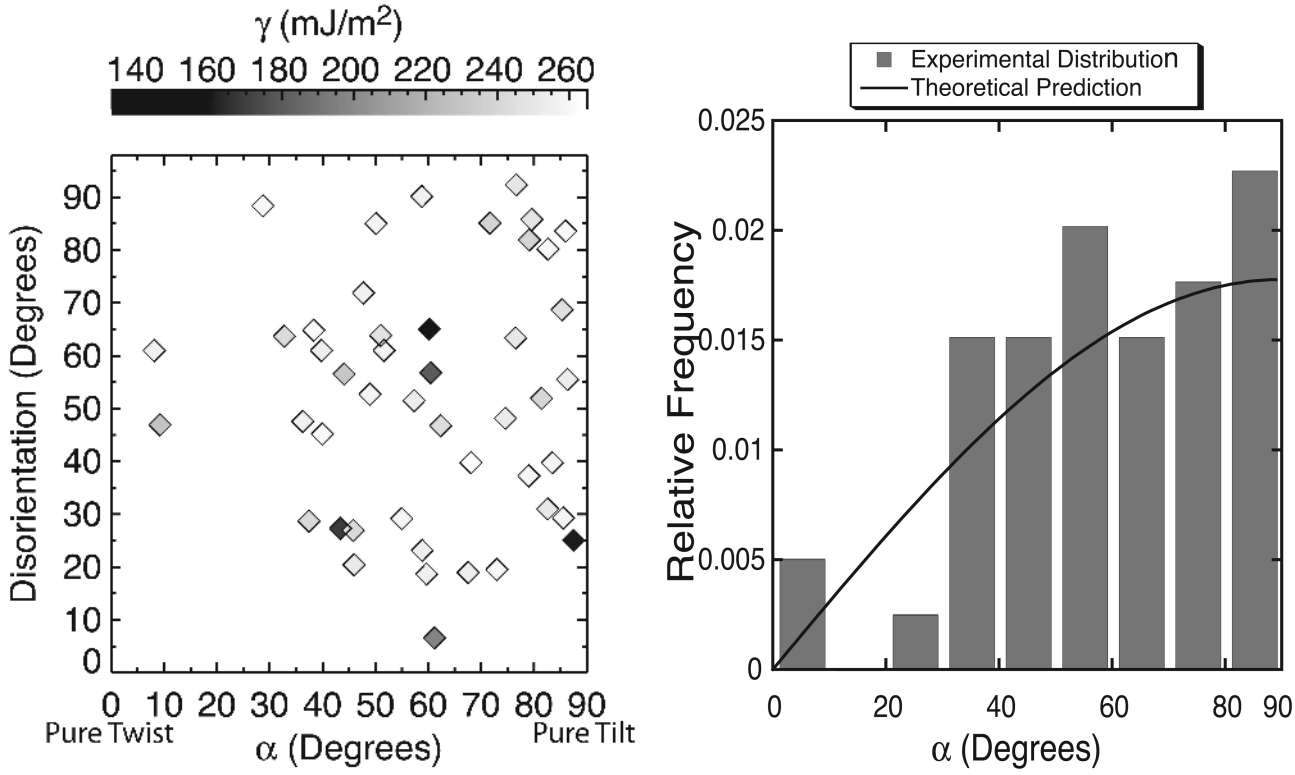

(*a*) (*b*)

Fig. 7—(*a*) Plot of the interfacial energy *vs* the disorientation angle, and α, which relates the degree of tilt and twist in the boundary. For $\alpha = 0$ deg, the boundary is a pure twist, and for $\alpha = 90$ deg, the boundary is a pure tilt. Low energies are shown as a dark point, and higher energies are shown as light point. (*b*) The probability of finding a value of α within the experimental data and a random sampling of grain boundaries.[30]

leading to a lower energy configuration, but it is impossible to detect this at the macroscopic level.

IV. CONCLUSIONS

The absolute grain boundary energy and the anisotropy are determined as a function of the crystallographic disorientation in Sn-1.3 at. pct Pb crystals. We find that two-thirds of the boundaries sampled were wetted with liquid and thus have an energy greater than 265 mJ/m^2. The measured grain boundary energies are much higher than reported previously, but we feel that this discrepancy is mainly due to surface contamination in the previous experiments. Grain boundaries with low energies exhibit an increased probability of occurrence when compared to boundaries formed by a random distribution of grain orientations. We find that the maximum torque term is significant for boundaries with relatively low interfacial energies, but that for most of the boundaries analyzed, this term can be safely ignored. We find that there are more tilt boundaries present within the sample than twist boundaries, and that most of the low energy boundaries have a mixed tilt-twist character.

ACKNOWLEDGMENT

The authors acknowledge financial support for this work by the Physical Sciences Division, NASA, and by the NASA Graduate Student Researchers Program Fellowship.

REFERENCES

1. A.D. Rollett, D.J. Srolovitz, and A. Karma: *Interface Sci*., 2002, vol. 10, pp. 119-19.
2. N.A. Gjostein and F.N. Rhines: *Acta Metall*., 1959, vol. 7, pp. 319-30.
3. G.C. Hasson and C. Goux: *Scripta Metall*., 1971, vol. 5 (10), pp. 889-94.
4. B.L. Adams, S. Ta'asan, D. Kinderlehrer, I. Livshits, D.E. Mason, C.T. Wu, W.W. Mullins, G.S. Rohrer, A.D. Rollett, and D.M. Saylor: *Interface Sci*., 1999, vol. 7, pp. 321-38.
5. D.M. Saylor, A. Morawiec, and G.S. Rohrer: *Acta Mater*., 2003, vol. 51, pp. 3663-74.
6. D.M. Saylor, A. Morawiec, and G.S. Rohrer: *Acta Mater*., 2003, vol. 51, pp. 3675-86.
7. M. Upmanyu, G.N. Hassold, A. Kazaryan, E.A. Holm, Y. Wang, B. Patton, and D.J. Srolovitz: *Interface Sci*., 2002, vol. 10, pp. 201-16.
8. A.D. Rollett: *Mater. Sci. Forum*., 2002, vol. 408 (4), pp. 251-56.
9. D.N. Wasnik, V. Kain, I. Samajdar, B. Verlinden, and P.K. De: *Acta Mater*., 2002, vol. 50, pp. 4587-4601.
10. C.A. Schuh, M. Kumar, and W.E. King: *Z. Metallkd*., 2003, vol. 94, pp. 323-28.
11. A.J. Schwartz and W.E. King: *JOM–J. Miner. Metall. Mater. Soc*., 1998, vol. 50, pp. 50-55.
12. D.M. Saylor, A. Morawiec, B.L. Adams, and G.S. Rohrer: *Interface Sci*., 2000, vol. 8, pp. 131-40.
13. C. Herring: *The Physics of Powder Metallurgy*, McGraw-Hill Book Co., New York, NY, 1951, p. 143.
14. H. Mykura: *Acta Metall*., 1955, vol. 3, p. 436.
15. W.T. Read and W. Shockley: *Phys. Rev*., 1950, vol. 78 (3), pp. 275-89.
16. T. Mori, H. Miura, T. Tokita, J. Haji, and M. Kato: *Phil. Mag*., 1988, vol. 58 (1), pp. 11-15.
17. S.C. Hardy and P.W. Voorhees: *Metall. Mater. Trans. A*, 1988, vol. 19A, pp. 2713-21.

18. V.A. Snyder, N. Akaiwa, J. Alkemper, and P.W. Voorhees: *Metall. Mater. Trans. A*, 1999, vol. 30, pp. 2341-48.
19. V.A. Snyder, J. Alkemper, and P.W. Voorhees: *Acta Mater.*, 2001, vol. 49 (4), pp. 599-709.
20. J. Alkemper, V. Snyder, N. Akaiwa, and P.W. Voorhees: *Phys. Rev. Lett.*, 1999, vol. 82 (13), pp. 2725-28.
21. D.W. Hoffman and J.W. Cahn: *Surf. Sci.*, 1972, vol. 31, pp. 368-88.
22. J.W. Cahn and D.W. Hoffman: *Acta Metall.*, 1974, vol. 22 (10), pp. 1205-14.
23. J. Alkemper and P.W. Voorhees: *J. Microsc.-Oxf.*, 2001, vol. 201, pp. 388-94.
24. T.L. Wolfsdorf-Brenner, P.W. Voorhees, and J. Sutliff: *Metall. Mater. Trans. A*, 1999, vol. 30A, pp. 1955-69.
25. M. Gündüz and J.D. Hunt: *Acta Metall.*, 1985, vol. 33, pp. 1651-72.
26. A. Heinz and P. Neumann: *Acta Crystallogr. A*, 1991, vol. A47, pp. 780-89.
27. A.U. Telang, T.R. Bieler, S. Choi, and K.N. Subramanian: *J. Mater. Res.*, 2002, vol. 17, pp. 2294-2306.
28. E.B. Greenhill and S.R. McDonald: *Nature*, 1953, vol. 171, p. 37.
29. Sui-Wai Chan and R.W. Balluffi: *Acta Metall.*, 1985, vol. 33 (6), pp. 1113-19.
30. A. Morawiec: *J. Appl. Cryst.*, 1995, vol. 28, pp. 289-93.
31. B.W. Krakauer and D.N. Seidman: *Acta Mater.*, 1998, vol. 46, pp. 6145-61.
32. T.L. Wolfsdorf, W.H. Bender, and P.W. Voorhees: *Acta Metall.*, 1997, vol. 45 (6), pp. 2279-95.